Journal of Materials Chemistry A

ROYAL SOCIETY OF CHEMISTRY

PAPER

View Article Online
View Journal | View Issue

Cite this: J. Mater. Chem. A, 2024, 12, 17557

C_6N_2S monolayer: an auxetic material with ultralow diffusion barrier and high storage capacity for potassium-ion batteries†

Jiayu Gao, ‡[a] Wenyuan Zhang, ‡[a] Aitor Bergara[bcd] and Guochun Yang *[ae]

Received 3rd April 2024
Accepted 7th June 2024

DOI: 10.1039/d4ta02238f

rsc.li/materials-a

The development of advanced anode materials is crucial for the applications of K-ion batteries (KIBs). In this study, swarm-intelligence structure search calculations have identified an auxetic C_6N_2S monolayer as a promising candidate with a desirable combination of storage capacity, rate capacity, and cycling endurance for KIBs. This monolayer exhibits a unique wavy structure, comprising S atoms forming valleys and interconnecting graphene-like nanoribbons forming peaks, with edge-sharing C_4N_2 rings. Its intrinsic metallicity, stemming from π-electron delocalization, facilitates favorable electronic conduction. The C_6N_2S monolayer spontaneously adsorbs two-layer K atoms, resulting in a stoichiometric composition of $C_6N_2SK_4$ and a high storage capacity of 812 mA h g^{-1}. The ultralow diffusion barrier of 0.03 eV along the valley ensures ultrafast ion transportation, while a moderate open circuit voltage of 0.28 V enhances battery safety. Furthermore, its auxetic behavior contributes to cycling stability. These remarkable properties of the C_6N_2S monolayer are attributed to its unique structural morphology and electron configuration induced by multiple-bond patterns.

1 Introduction

The escalating energy demand in contemporary society has led to a pressing need for alternative energy sources. However, traditional nonrenewable fossil fuels are facing depletion, prompting the search for sustainable alternatives. Although lithium-ion batteries (LIBs) have long been the frontrunner in energy storage technology,[1,2] they alone cannot meet the future energy demands. As a solution, potassium-ion batteries (KIBs) have emerged as a promising option. Leveraging the advancements of LIB technologies and materials, KIBs offer several advantages, including the abundance of potassium, a low K/K^+ redox potential, and the similarity in chemistry to lithium.[3–5] Despite these advantages, the practical development of KIBs faces a critical challenge: the identification of high-performance anode materials.[6,7] Addressing this challenge is crucial for the widespread adoption and success of KIB technology.

Carbonaceous materials, including graphite, soft carbon, and hard carbon, stand as the most prevalent anode materials for LIBs due to their exceptional performance, wide availability, and robust stability.[8–10] Graphite, particularly, has emerged as a commercial anode material for LIBs, showcasing a remarkable storage capacity of 372 mA h g^{-1}, coupled with enduring cycling stability, and high rate capacity.[11] However, when it comes to KIBs, graphite falls short, offering a lower storage capacity of 273 mA h g^{-1}, sluggish K^+ diffusion kinetics, and increased charge transfer resistance due to the larger atomic mass and ionic radius of K^+.[12,13] In response, various strategies such as doping, grafting, and structural engineering have been explored to augment the storage capacity and enhance the electrochemical performance of carbon-based materials for KIBs.[14–17]

Numerous two-dimensional (2D) materials have showcased remarkable electrochemical performance for metal-ion batteries (MIBs), owing to their high active site density, short ion diffusion length, and excellent electrical conductivity.[18–20] Graphene, being the quintessential 2D material, boasts exceptional structural stability, outstanding charge transport capabilities, and a perfect planar geometry. However, it is not an optimal choice for KIBs, with a maximum capacity of only 230 mA h g^{-1} and a capacity retention of 66%,[21,22] primarily due to its delocalized π electrons dominated by sp^2 hybridization. Nonetheless, the electrochemical properties and storage capacity of graphene can be tailored to some extent through

[a]State Key Laboratory of Metastable Materials Science & Technology and Key Laboratory for Microstructural Material Physics of Hebei Province, School of Science, Yanshan University, Qinhuangdao 066004, China

[b]Physics Department and EHU Quantum Center, Universidad del País Vasco-Euskal Herriko Unibertsitatea, UPV/EHU, 48080 Bilbao, Spain

[c]Donostia International Physics Center (DIPC), 20018 Donostia, Spain

[d]Centro de Física de Materiales CFM, Centro Mixto CSIC-UPV/EHU, 20018 Donostia, Spain

[e]Centre for Advanced Optoelectronic Functional Materials Research and Key Laboratory for UV Light-Emitting Materials and Technology of Ministry of Education, Northeast Normal University, Changchun 130024, China. E-mail: yanggc468@nenu.edu.cn

† Electronic supplementary information (ESI) available. See DOI: https://doi.org/10.1039/d4ta02238f

‡ Jiayu Gao and Wenyuan Zhang are co-first-authors.

heteroatom doping (*e.g.* N, P, O, and S).[23] Conversely, certain C-rich 2D materials, such as C_3N,[24] BC_3,[25] and TiC_3,[26] have demonstrated superior performance as anodes for MIBs.

Taking into account the limitations of traditional carbonaceous materials and the potential of 2D materials for improving the performance of potassium-ion batteries (KIBs), we propose a novel strategy centered around the integration of electron-rich nitrogen and sulfur atoms to regulate the structural morphologies and orbital hybridizations/occupancies of carbon-rich 2D materials. Herein, we also combine the high stability of the C_3N monolayer[27] with the improved conductivity by doping it with a small amount of S atoms. This approach is intended to develop high-performance anode materials for KIBs. Therefore, we conduct a structural search on the chemical ratio of multiplex cell C_3N doped single S, and evaluate its stability for screening. Through this approach, we have identified a promising candidate: the C_6N_2S monolayer. This material exhibits a suite of desirable properties for KIBs, including a high theoretical capacity of 812 mA h g^{-1}, an ultralow diffusion barrier of 0.03 eV, a low average open circuit voltage (OCV) of 0.28 V, and an excellent electronic conduction and mechanical stability. Our study presents a compelling avenue for the development of high-performance anode materials for KIBs.

2 Computational details

The swarm-intelligence structure search method[28–30] was employed to explore the low-energy structures of the ternary C–N–S system. This method is effective in identifying stable and metastable structures, making it instrumental in the discovery of new materials.[31–34] The structural relaxation and property calculations were conducted using density functional theory as implemented in the Vienna *Ab initio* Simulation Package.[35] The Perdew–Burke–Ernzerhof (PBE) functional within the generalized gradient approximation was utilized for these calculations.[36] A plane-wave cut-off energy of 600 eV, a force convergence of 0.001 eV $Å^{-1}$, and an energy convergence of 10^{-5} eV were employed to ensure accuracy. Additionally, a vacuum layer of 20 Å was included to prevent interactions between layers in the 2D structure. The dynamic stability of the predicted structures was verified by calculating the phonon dispersion curve using the supercell method implemented in the Phonopy code.[37] Furthermore, *ab initio* molecular dynamics simulations (AIMD) were performed at 500 K to evaluate the thermal stability of the structures.[38] Finally, the diffusion barriers of metal ions on the predicted monolayer were estimated using the nudged elastic band method.[39]

The adsorption energy of a K ion on the C_6N_2S monolayer was computed using the following formula:

$$\mathrm{E_{ad}} = \frac{\left(E_{C_6N_2SK_n} - E_{C_6N_2S} - nE_K\right)}{n} \quad (1)$$

where E_{C_6N2SKn} is the total energy of the C_6N_2S monolayer with adsorbed K atoms, $E_{C_6N_2S}$ is the energy of the pristine C_6N_2S monolayer, E_K is the energy of a K atom in the body-centered cubic (bcc) structure, and n is the number of the adsorbed K atoms.

In the charge and discharge process, the average open circuit voltage (OCV) was obtained based on the equation below:

$$V_{ave} = \frac{\Delta E}{nzF} = \frac{E_{C_6N_2S} + nE_K - E_{C_6N_2SK_n}}{nzF} \quad (2)$$

where z is the electronic charge of the adsorbed ion in the electrolyte and F is the Faraday constant (26.8 A h mol^{-1}).

The theoretical specific capacity was evaluated with the following equation:

$$C = \frac{nF}{W} \quad (3)$$

where W is the molecular weight of the C_6N_2S monolayer.

3 Results and discussion

3.1 Structure and stability

The C_6N_2S monolayer exhibits a distinctive wave-like structure with the space group *Pmm*2, characterized by its unit cell containing twelve C, four N, and two S atoms. Notably, there are three distinct three-coordinated environments for C atoms: a C atom forming bonds with two neighboring C atoms and one S atom, a C atom coordinated with two neighboring N atoms and one C atom, and a C atom linked to two neighboring C atoms and one N atom. Each N atom is coordinated with three neighboring C atoms. These arrangements result in sp^2 hybridization of C and N atoms, forming graphene-like nanoribbons with edge-sharing C_4N_2 rings. The zigzag C chains in the nanoribbons align along the *a*-axis direction due to the C richness. S atoms, on the other hand, are two-coordinated with C atoms in different zigzag chains, exhibiting sp^3 hybridization, as observed in the C_2S monolayer (Fig. 1a).[40] The non-bonding electrons of S atoms form lone-electron pairs, contributing to the formation of a valley along the *a*-axis direction between S atoms and zigzag C chains. All atoms in the C_6N_2S monolayer satisfy the octet rule, and the corresponding bonds exhibit typical covalence (Fig. 1b). The average bond lengths of C–C, C–N, and C–S are 1.38 Å, 1.43 Å, and 1.76 Å, respectively, closely resembling those observed in graphene (1.42 Å),[41] C_3N (1.40 Å),[42] and C_3S (1.78 Å)[43] structures.

The energetic, dynamic, thermal, and mechanical stability of the C_6N_2S monolayer was assessed to explore its synthesis and application potential. Its cohesive energy, calculated at 8.01 eV/atom, exceeds that of the C_3N (7.08 eV per atom)[44] and C_3S (7.26 eV per atom)[43] monolayers, indicating a relatively high stability. Molecular dynamics simulations at 500 K for 10 ps revealed that its initial structural configuration remained intact without any chemical bond breaking, confirming its thermal stability (Fig. 1c). The dynamic stability of the C_6N_2S monolayer was verified using positive phonon frequencies across all vibrational modes, with the highest phonon frequency reaching 1486 cm^{-1}, indicative of strong covalent bonds (Fig. 1d). Elastic constants calculated for the material meet the Born–Huang criterion, confirming its mechanical stability (Table S2†). These high stabilities suggest that the C_6N_2S monolayer could feasibly be synthesized under certain conditions. Interestingly, the monolayer exhibits anisotropic mechanical behavior, as evidenced by

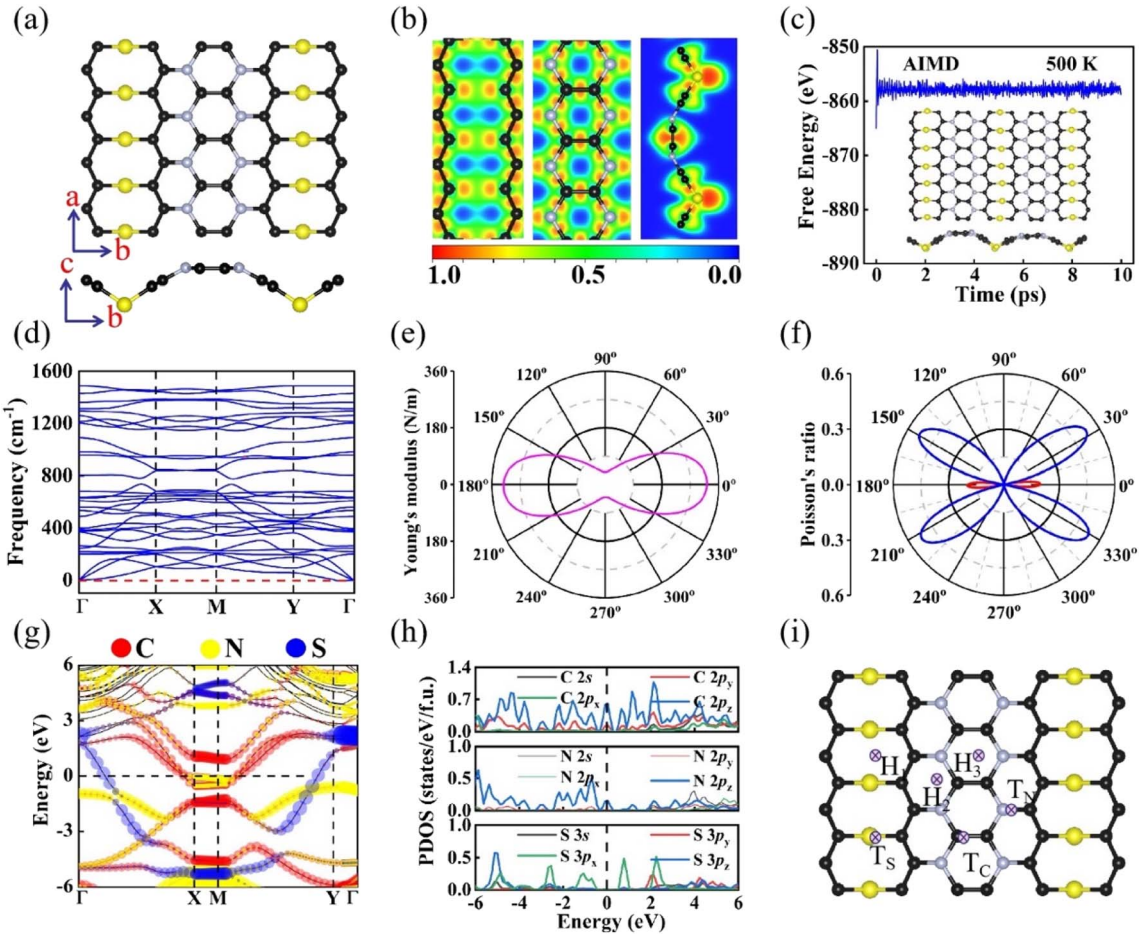

Fig. 1 (a) Top and side views of the crystal structure of the predicted C_6N_2S monolayer, where black, gray, and yellow balls represent C, N, and S atoms, respectively. Its structural parameters can be found in Table S1.† (b) The electron localization function (ELF) map, (c) the AIMD at 500 K with the free-energy evolution and final structure, (d) the phonon dispersion curves, (e) the Young's modulus, and (f) the Poisson's ratio, where blue and red lines represent positive and negative values, respectively. (g) The projected electronic band structure, (h) PDOS, and (i) the selected adsorption sites of the C_6N_2S monolayer.

its Young's modulus, which reaches a maximum value of 322.8 N m^{-1} along the *a*-axis direction (Fig. 1e). Furthermore, its Poisson's ratio ranges from −0.53 to 0.20, as illustrated in Fig. 1f. Materials with negative Poisson's ratio have been considered valuable for applications in aerospace and defense areas due to their unique transverse contraction or expansion under uniaxial pressure or tension.[45] Additionally, materials with negative Poisson's ratio serve as electrodes in MIBs, suppressing volume expansion and enhancing flexibility during charge and discharge processes.[46,47]

3.2 Electronic properties

The electronic properties of the C_6N_2S monolayer were investigated through electronic band structure and projected density of states (PDOS) calculations at the PBE level. The analysis revealed that the C_6N_2S monolayer exhibits metallic behavior, evidenced by the presence of three bands crossing the Fermi level (Fig. 1g). Its intrinsic metallicity is also confirmed using the HSE06 functional (Fig. S1†). The metallic character arises from the delocalized π electrons contributed by the C 2p$_z$ and N 2p$_z$ states (Fig. 1h). The presence of delocalized π electrons ensures rapid contact of electron carriers with intercalation ions,[48] a desirable property for metal-ion anode materials. Of the five valence electrons of N atom, three participate in in-plane covalent bonds *via* sp^2 hybridization, while the remaining two electrons, symmetrically distributed out of plane, form π bonds with the C 2p$_z$ electrons.

3.3 Electrochemical performance as an anode material

The C_6N_2S monolayer exhibits auxetic behavior and intrinsic metallicity, making it favorable for MIB anodes. To assess its feasibility, we investigate its adsorption ability, diffusion energy barrier, storage capacity, and open circuit voltage (OCV) for alkali metal ions (*e.g.*, Li, Na, and K), crucial for anode materials. We consider six inequivalent adsorption sites on the C_6N_2S monolayer (Fig. 1i). The $H_1/H_2/H_3$ sites are located at the hollows (H) of the octagonal C_6S_2 ring or two different hexagonal C_4N_2 rings, while the $T_C/T_N/T_S$ represent the top (T) site directly above a C/N/S atom. Among these, H_1 emerges as the most favorable adsorption site for Li, Na, and K ions.

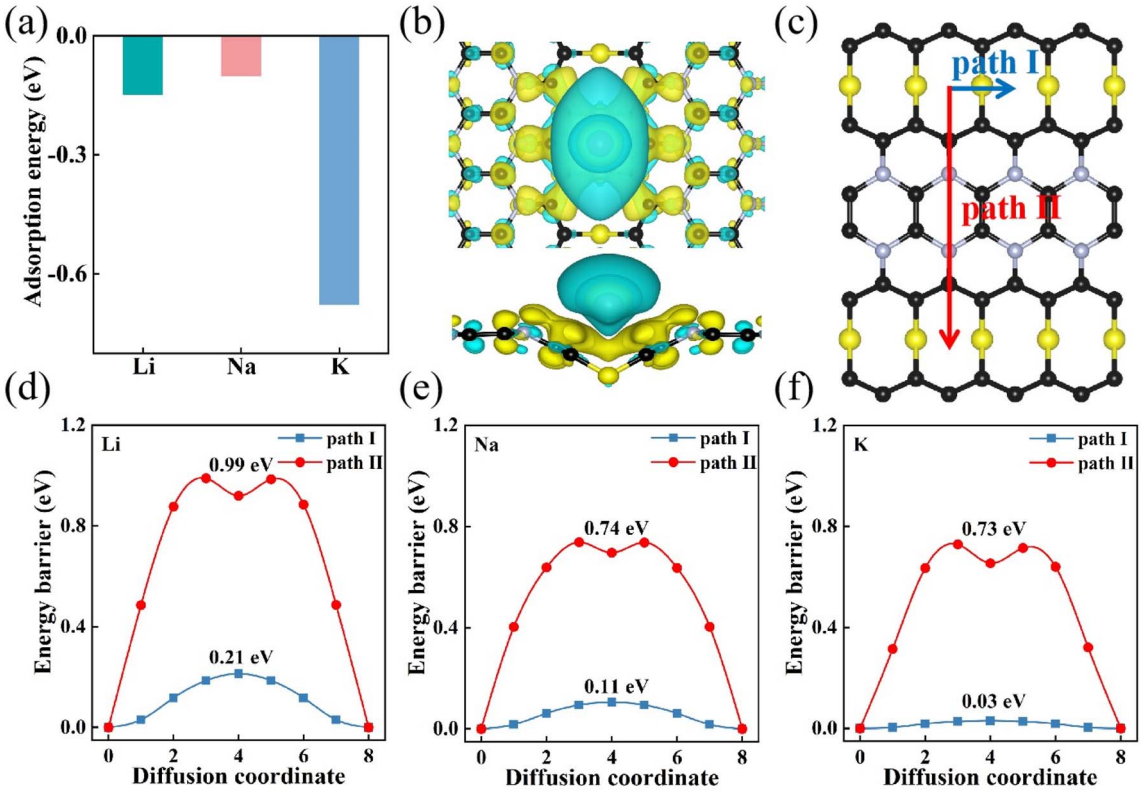

Fig. 2 (a) The calculated adsorption energies of Li, Na, and K on the H_1 site of the C_6N_2S monolayer. (b) The top and side views of the charge density difference when K is adsorbed on the C_6N_2S monolayer. (c) Two ion-migration paths on the C_6N_2S monolayer, with blue and red arrows indicating paths I and II, respectively. (d–f) The migration barriers of Li, Na, K ions across the two paths.

Specifically, the C_6N_2S monolayer exhibits the strongest adsorption ability for K atoms, with an adsorption energy of −0.68 eV (Fig. 2a). This value is conducive to preventing the formation of K clusters, thereby enhancing battery safety. The adsorption process induces an evident charge transfer from the K atom to the C_6N_2S monolayer, as indicated by the charge depletion around the metal atom (blue region) and the charge accumulation on the monolayer (yellow region) (Fig. 2b and S2†), indicative of chemical adsorption (Fig. S3†).

The ion-migration energy barrier directly influences the rate performance in the charge/discharge process.[49] Lower migration energy barriers generally correspond to higher rate capacities. Considering the favorable adsorption site of H_1 and unique atomic arrangement, there are two potential diffusion pathways: path I and path II. As shown in Fig. 2c, path I follows a V-shape channel constructed by S atoms interconnecting zigzag C chains, while path II involves movement from H_1 to adjacent C_4N_2 hexatomic rings before returning to H_1. As illustrated in Fig. 2d–f, path I is favorable for the transportation of Li, Na, and K ions. Notably, the barrier for K ions (0.03 eV) is significantly lower than that for Li (0.21 eV) and Na (0.11 eV). Compared to the other 2D materials such as PC_6 (0.26 eV),[50] Si_3C (0.18 eV),[51] and BiC (0.14 eV),[52] the C_6N_2S monolayer exhibits excellent ion transportation ability. Particularly, the diffusion of K ions along the V-shape channel is virtually barrier-free, indicating an exceptionally high rate performance for KIBs.

Subsequently, we focus on exploring the performance of the C_6N_2S monolayer as a KIB anode material. The storage capacity of an anode material is linearly correlated with the number of adsorbed K atoms. To simulate the adsorption process, we utilize a $3 \times 2 \times 1$ supercell to investigate four different K concentrations (*i.e.*, $C_6N_2SK_n$, n = 1–4). The stable configurations for the four considered stoichiometries are depicted in Fig. 3a–d. The corresponding adsorption energies are −0.45 eV, −0.26 eV, −0.22 eV, and −0.15 eV, indicating favorable K ion adsorption on the C_6N_2S monolayer. The adsorption energy gradually increases with K ion concentrations due to the enhanced electrostatic repulsion between K ions. As expected, the stoichiometry of $C_6N_2SK_4$ corresponds to a theoretical capacity of 812 mA h g^{-1}, significantly higher than that of typical 2D materials such as Ti_3C_2 (191.8 mA h g^{-1}),[53] GeSe (353.65 mA h g^{-1}),[54] and BP (570 mA h g^{-1}).[55]

An excellent anode material also requires subtle structural changes during the charge/discharge process. It is noted that the C_6N_2S monolayer in $C_6N_2SK_n$ (n = 1–4) conformers preserves its initial configuration, showing minor changes in structural parameters (Table S3†), which is favorable for reducing cycle instability and capacity loss. To explore the structural flexibility of C_6N_2S, we chose to remove adsorbed K from the $C_6N_2SK_4$ and perform structural relaxation of the twisted C_6N_2S structure. According to Fig. S4,† the C_6N_2S structure is completely restored to its original configuration. It is worth noting that the four stable adsorption structures still demonstrate metallicity

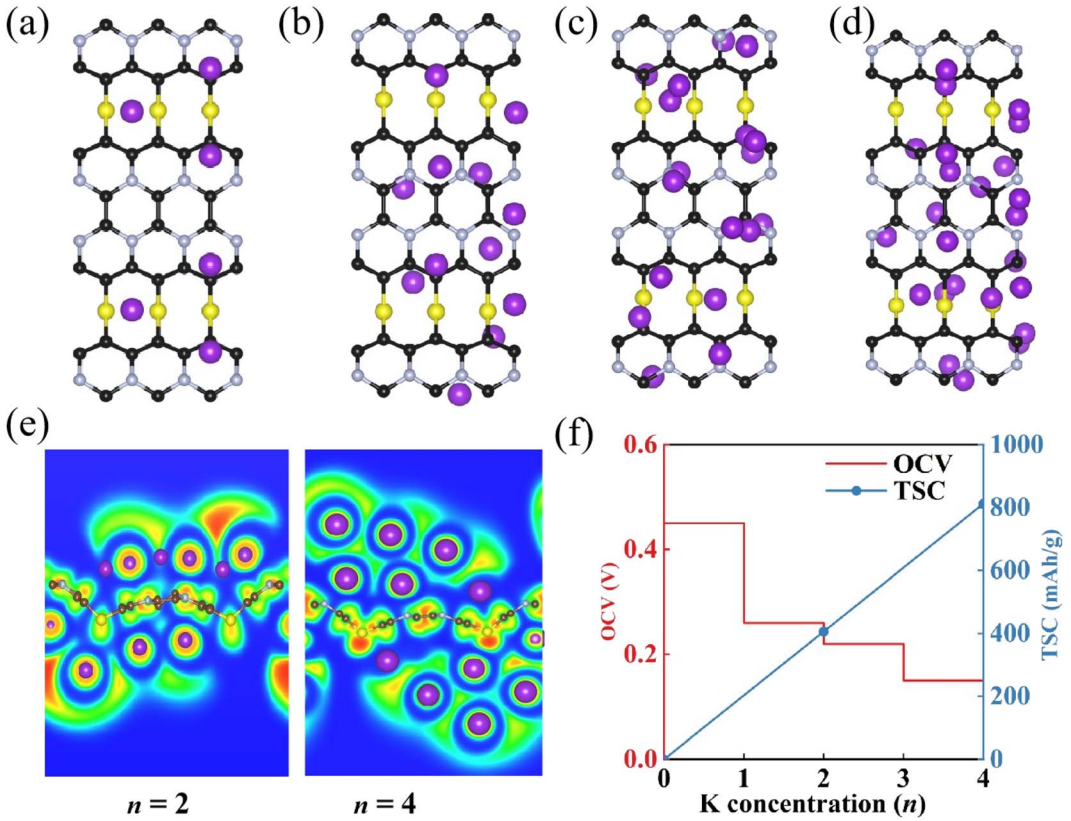

Fig. 3 (a–d) The most stable structures with different K concentrations in $C_6N_2SK_n$ ($n = 1$–4) with the adsorbed atom number of 6, 12, 18, and 24, respectively. (e) The ELF map of $C_6N_2SK_n$ ($n = 2$ and 4). (f) OCV and theoretical capacity (TSC) as a function of the K concentration.

(Fig. S5†), providing high electrical conductivity during battery cycles. For the C_6N_2S monolayer, its high storage capacity can be attributed to several factors. Firstly, the large electronegativity difference between K atoms and the constituent atoms of the C_6N_2S monolayer favors strong adsorption. Secondly, the dispersed intra- and inter-layer anionic electrons reduce electrostatic repulsion between K atoms, favoring the multilayer adsorption (Fig. 3e).

The OCV is a vital performance parameter to evaluate the battery safety of anode materials. For KIBs, an OCV ranging from 0.0 V to 1.0 V can avoid dendrite formation of K atoms during the discharge/charge process.[56] We explore the OCV evolution associated with K ion concentration. As illustrated in Fig. 3f, with increasing adsorption concentration, the resultant OCV gradually decreases from 0.45, 0.26, 0.22, to 0.15 V, indicating that the variation of K intercalation voltage is steady and meets the safety requirement of KIBs. Additionally, the calculated average OCV is 0.28 V, which is much lower than that of other 2D materials such as SnS_2 (0.84 V)[57] and AlP (0.71 V).[58] These outstanding properties render the C_6N_2S monolayer a promising candidate for KIB anode applications.

To further evaluate the performance of the C_6N_2S structure in practical applications, we construct four bilayer stackings: (a) aligned stacking, (b) *a*-direction translational stacking, (c) *b*-direction translational stacking, and (d) simultaneous translational stacking along the *a* and *b* directions, as shown in Fig. S6.† After the optimization, we select the lowest energy structure with *a*-direction translational stacking to study its ability in storing K. The bilayer C_6N_2S can still adsorb 24 K atoms, corresponding to a theoretical capacity of 406 mA h g^{-1}.

4 Conclusions

Based on our control of structural topologies and orbital occupancies through chemical compositions, we have discovered a novel C-rich C_6N_2S monolayer with a wave-like structure using first-principles swarm-intelligence structural search calculations. Our study of its structure reveals excellent stability attributed to sp^3-hybridized C–S and sp^2-hybridized C–N/C–C covalent bonds that satisfy the chemical octet rule. The C_6N_2S monolayer shows promising potential for application in potassium-ion batteries (KIBs) due to several key characteristics. It exhibits an ultralow diffusion barrier of 0.03 eV, indicating fast ion transport, along with a high theoretical capacity of 812 mA h g^{-1}. Additionally, it possesses a desirable average open circuit voltage (OCV) of 0.28 V. Notably, its auxetic behavior, stemming from its wave-like structure, offers additional mechanical stability during the charge/discharge process. Our work provides a strategic approach for the development of C-rich 2D anode materials, addressing the current shortage of high-performance anode materials for KIBs. This research opens avenues for the design and synthesis, contributing to the advancement of KIB technology.

Data availability

Data will be made available on request.

Conflicts of interest

The authors declare that they have no known competing financial interests or personal relationships that could have appeared to influence the work reported in this paper.

Acknowledgements

The authors acknowledge funding from the Natural Science Foundation of China under Grant No. 22372142, 12304028, and U23A20537, the High-End Foreign Expert Introduction Program (G2023003004L), the Central Guiding Local Science and Technology Development Fund Projects (236Z7605 G), the Natural Science Foundation of Hebei Province (Grant No. B2021203030), and the Science and Technology Project of Hebei Education Department (JZX2023020). A. B. acknowledges financial support from the Spanish Ministry of Science and Innovation (Grant No. PID2022-139230NB-I00) and the Department of Education, Universities and Research of the Basque Government and the University of the Basque Country (Grant No. IT1707-22). This work was carried out at the National Supercomputer Center in Tianjin, and the calculations were performed on TianHe-1 (A).

References

1 X. Shu, L. Hu, T. Heine and Y. Jing, Rational molecular design of redox-active carbonyl-bridged heterotriangulenes for high-performance lithium-ion batteries, *Adv. Sci.*, 2024, **11**, e2306680.
2 T. Xu, Y. Yang, T. Liu and Y. Jing, Two-dimensional covalent organic frameworks made of triquinoxalinylene derivatives are promising anodes for high-performance lithium and sodium ion batteries, *RSC Adv.*, 2023, **13**, 34724–34732.
3 T. Hosaka, K. Kubota, A. S. Hameed and S. Komaba, Research development on K-ion batteries, *Chem. Rev.*, 2020, **120**, 6358–6466.
4 D. Larcher and J.-M. Tarascon, Towards greener and more sustainable batteries for electrical energy storage, *Nat. Chem.*, 2015, **7**, 19–29.
5 X. Min, J. Xiao, M. Fang, W. Wang, Y. Zhao, Y. Liu, A. M. Abdelkader, K. Xi, R. V. Kumar and Z. Huang, Potassium-ion batteries: outlook on present and future technologies, *Energy Environ. Sci.*, 2021, **14**, 2186–2243.
6 W. Zhang, Y. Liu and Z. Guo, Approaching high-performance potassium-ion batteries via advanced design strategies and engineering, *Sci. Adv.*, 2019, **5**, eaav7412.
7 C. Chi, Z. Liu, X. Lu, Y. Meng, C. Huangfu, Y. Yan, Z. Qiu, B. Qi, G. Wang, H. Pang, T. Wei and Z. Fan, Balance of sulfur doping content and conductivity of hard carbon anode for high-performance K-ion storage, *Energy Storage Mater.*, 2023, **54**, 668–679.
8 X. Wu, Y. Chen, Z. Xing, C. W. K. Lam, S. S. Pang, W. Zhang and Z. Ju, Advanced carbon-based anodes for potassium-ion batteries, *Adv. Energy Mater.*, 2019, **9**, 1900343.
9 S. Z. Butler, S. M. Hollen, L. Cao, Y. Cui, J. A. Gupta, H. R. Gutiérrez, T. F. Heinz, S. S. Hong, J. Huang, A. F. Ismach, E. Johnston-Halperin, M. Kuno, V. V. Plashnitsa, R. D. Robinson, R. S. Ruoff, S. Salahuddin, J. Shan, L. Shi, M. G. Spencer, M. Terrones, W. Windl and J. E. Goldberger, Progress, challenges, and opportunities in two-dimensional materials beyond graphene, *ACS Nano*, 2013, **7**, 2898–2926.
10 Y. Shi, G. Liu, R. Jin, H. Xu, Q. Wang and S. Gao, Carbon materials from melamine sponges for supercapacitors and lithium battery electrode materials: a review, *Carbon Energy*, 2019, **1**, 253–275.
11 Y. Wen, K. He, Y. Zhu, F. Han, Y. Xu, I. Matsuda, Y. Ishii, J. Cumings and C. Wang, Expanded graphite as superior anode for sodium-ion batteries, *Nat. Commun.*, 2014, **5**, 4033.
12 M. Sha, L. Liu, H. Zhao and Y. Lei, Anode materials for potassium-ion batteries: current status and prospects, *Carbon Energy*, 2020, **2**, 350–369.
13 W. Zhang, Y. Liu and Z. Guo, Approaching high-performance potassium-ion batteries via advanced design strategies and engineering, *Sci. Adv.*, 2019, **5**, eaav7412.
14 J. Ding, H. Zhang, H. Zhou, J. Feng, X. Zheng, C. Zhong, E. Paek, W. Hu and D. Mitlin, Sulfur-grafted hollow carbon spheres for potassium-ion battery anodes, *Adv. Mater.*, 2019, **31**, 1900429.
15 K. Share, A. P. Cohn, R. Carter, B. Rogers and C. L. Pint, Role of nitrogen-doped graphene for improved high-capacity potassium ion battery anodes, *ACS Nano*, 2016, **10**, 9738–9744.
16 C. Yang, X. Liang, X. Ou, Q. Zhang, H.-S. Zheng, F. Zheng, J.-H. Wang, K. Huang and M. Liu, Heterostructured nanocube-shaped binary sulfide $(SnCo)S_2$ interlaced with S-doped graphene as a high-performance anode for advanced Na^+ batteries, *Adv. Funct. Mater.*, 2019, **29**, 1807971.
17 B. Wang, Z. Zhang, F. Yuan, D. Zhang, Q. Wang, W. Li, Z. Li, Y. A. Wu and W. Wang, An insight into the initial coulombic efficiency of carbon-based anode materials for potassium-ion batteries, *Chem. Eng. J.*, 2022, **428**, 131093.
18 X. Wang, S. Kajiyama, H. Iinuma, E. Hosono, S. Oro, I. Moriguchi, M. Okubo and A. Yamada, Pseudocapacitance of MXene nanosheets for high-power sodium-ion hybrid capacitors, *Nat. Commun.*, 2015, **6**, 6544.
19 J. Lin, T. Yu, F. Han and G. Yang, Computational predictions of two-dimensional anode materials of metal-ion batteries, *Wiley Interdiscip. Rev.: Comput. Mol. Sci.*, 2020, **10**, e1473.
20 S. Mukherjee and G. Singh, Two-dimensional anode materials for non-lithium metal-ion batteries, *ACS Appl. Energy Mater.*, 2019, **2**, 932–955.
21 Z. Tai, Y. Liu, Q. Zhang, T. Zhou, Z. Guo, H. K. Liu and S. X. Dou, Ultra-light and flexible pencil-trace anode for high performance potassium-ion and lithium-ion batteries, *Green Energy Environ.*, 2017, **2**, 278–284.

22 A. K. Geim, Graphene: status and prospects, *Science*, 2009, **324**, 1530–1534.
23 A. Ambrosi, C. K. Chua, A. Bonanni and M. Pumera, Electrochemistry of graphene and related materials, *Chem. Rev.*, 2014, **114**, 7150–7188.
24 P. Bhauriyal, A. Mahata and B. Pathak, Graphene-like carbon–nitride monolayer: a potential anode material for Na-and K-ion batteries, *J. Phys. Chem. C*, 2018, **122**, 2481–2489.
25 R. P. Joshi, B. Ozdemir, V. Barone and J. E. Peralta, Hexagonal BC_3: A robust electrode material for Li, Na, and K ion batteries, *J. Phys. Chem. Lett.*, 2015, **6**, 2728–2732.
26 T. Yu, Z. Zhao, L. Liu, S. Zhang, H. Xu and G. Yang, TiC_3 monolayer with high specific capacity for sodium-ion batteries, *J. Am. Chem. Soc.*, 2018, **140**, 5962–5968.
27 S. Yang, W. Li, C. Ye, G. Wang, H. Tian, C. Zhu, P. He, G. Ding, X. Xie, Y. Liu, Y. Lifshitz, S. T. Lee, Z. Kang and M. Jiang, C_3N-A 2D crystalline, hole-free, tunable-narrow-bandgap semiconductor with ferromagnetic properties, *Adv. Mater.*, 2017, **29**, 1605625.
28 Y. Wang, J. Lv, L. Zhu and Y. Ma, Crystal structure prediction via particle-swarm optimization, *Phys. Rev. B*, 2010, **82**, 094116.
29 X. Luo, J. Yang, H. Liu, X. Wu, Y. Wang, Y. Ma, S.-H. Wei, X. Gong and H. Xiang, Predicting two-dimensional boron–carbon compounds by the global optimization method, *J. Am. Chem. Soc.*, 2011, **133**, 16285–16290.
30 X. Shao, J. Lv, P. Liu, S. Shao, P. Gao, H. Liu, Y. Wang and Y. Ma, A symmetry-orientated divide-and-conquer method for crystal structure prediction, *J. Chem. Phys.*, 2022, **156**, 014105.
31 S. Zhao, Z. Li and J. Yang, Obtaining two-dimensional electron gas in free space without resorting to electron doping: an electride based design, *J. Am. Chem. Soc.*, 2014, **136**, 13313–13318.
32 J. Guan, D. Liu, Z. Zhu and D. Tománek, Two-dimensional phosphorus carbide: Competition between sp^2 and sp^3 bonding, *Nano Lett.*, 2016, **16**, 3247–3252.
33 G. Wang, R. Pandey and S. P. Karna, Carbon phosphide monolayers with superior carrier mobility, *Nanoscale*, 2016, **8**, 8819–8825.
34 K. A. Tikhomirova, C. Tantardini, E. V. Sukhanova, Z. I. Popov, S. A. Evlashin, M. A. Tarkhov, V. L. Zhdanov, A. A. Dudin, A. R. Oganov and D. G. Kvashnin, Exotic two-dimensional structure: the first case of hexagonal NaCl, *J. Phys. Chem. Lett.*, 2020, **11**, 3821–3827.
35 G. Kresse and J. Furthmüller, Efficient iterative schemes for ab initio total-energy calculations using a plane-wave basis set, *Phys. Rev. B*, 1996, **54**, 11169.
36 J. P. Perdew, K. Burke and M. Ernzerhof, Generalized gradient approximation made simple, *Phys. Rev. Lett.*, 1996, **77**, 3865.
37 A. Togo, F. Oba and I. Tanaka, First-principles calculations of the ferroelastic transition between rutile-type and $CaCl_2$-type SiO_2 at high pressures, *Phys. Rev. B*, 2008, **78**, 134106.
38 A. Togo and I. Tanaka, First principles phonon calculations in materials science, *Scr. Mater.*, 2015, **108**, 1–5.
39 G. Mills and H. Jónsson, Quantum and thermal effects in H_2 dissociative adsorption: Evaluation of free energy barriers in multidimensional quantum systems, *Phys. Rev. Lett.*, 1994, **72**, 1124–1127.
40 M. Tang, U. Schwingenschlögl and G. Yang, The metallic C_6S monolayer with high specific capacity for K-ion batteries, *Mater. Today Chem.*, 2022, **25**, 100951.
41 M. F. Budyka, T. S. Zyubina, A. G. Ryabenko, S. H. Lin and A. M. Mebel, Bond lengths and diameters of armchair single wall carbon nanotubes, *Chem. Phys. Lett.*, 2005, **407**, 266–271.
42 A. Bafekry, S. Farjami Shayesteh and F. M. Peeters, C_3N monolayer: Exploring the emerging of novel electronic and magnetic properties with adatom adsorption, functionalizations, electric field, charging, and strain, *J. Phys. Chem. C*, 2019, **123**, 12485–12499.
43 M. Tang, B. Wang, H. Lou, F. Li, A. Bergara and G. Yang, Anisotropic and high-mobility C_3S monolayer as a photocatalyst for water splitting, *J. Phys. Chem. Lett.*, 2021, **12**, 8320–8327.
44 L. Xie, L. Yang, W. Ge, X. Wang and J. Jiang, Bandgap tuning of C_3N monolayer: A first-principles study, *Chem. Phys.*, 2019, **520**, 40–46.
45 C. Huang and L. Chen, Negative Poisson's ratio in modern functional materials, *Adv. Mater.*, 2016, **28**, 8079–8096.
46 L. Weng, C. Xu, B. Chen, J. Zhou, R. Cai and Y. Shi, A comparative study on ratcheting deformation between negative Poisson's ratio electrode and thin film electrode in Li-ion battery cyclic operation, *Mech. Mater.*, 2020, **150**, 103567.
47 L. Weng, J. Zhou and R. Cai, Analytical model of Li-ion diffusion-induced stress in nanowire and negative Poisson's ratio electrode under different operations, *Int. J. Mech. Sci.*, 2018, **141**, 245–261.
48 L. Li, D. Zhang, J. Deng, Y. Gou, J. Fang, H. Cui, Y. Zhao and M. Cao, Carbon-based materials for fast charging lithium-ion batteries, *Carbon*, 2021, **183**, 721–734.
49 B. Tian, W. Du, L. Chen, J. Guo, H. Shu, Y. Wang and J. Dai, Probing pristine and defective NiB_6 monolayer as promising anode materials for Li/Na/K ion batteries, *Appl. Surf. Sci.*, 2020, **527**, 146580.
50 K. Dou, Y. Ma, T. Zhang, B. Huang and Y. Dai, Prediction of two-dimensional PC_6 as a promising anode material for potassium-ion batteries, *Phys. Chem. Chem. Phys.*, 2019, **21**, 26212–26218.
51 Y. Wang and Y. Li, Ab initio prediction of two-dimensional Si_3C enabling high specific capacity as an anode material for Li/Na/K-ion batteries, *J. Mater. Chem. A*, 2020, **8**, 4274–4282.
52 A. Ghani, S. Ahmed, A. Murtaza, I. Muhammad, W. u. Rehman, C. Zhou, W. L. Zuo and S. Yang, Bi–C monolayer as a promising 2D anode material for Li, Na, and K-ion batteries, *Phys. Chem. Chem. Phys.*, 2023, **25**, 4980–4986.
53 D. Er, J. Li, M. Naguib, Y. Gogotsi and V. B. Shenoy, Ti_3C_2 MXene as a high capacity electrode material for metal (Li,

Na, K, Ca) ion batteries, *ACS Appl. Mater. Interfaces*, 2014, **6**, 11173–11179.

54 Y. Zhou, M. Zhao, Z. W. Chen, X. M. Shi and Q. Jiang, Potential application of 2D monolayer β-GeSe as an anode material in Na/K ion batteries, *Phys. Chem. Chem. Phys.*, 2018, **20**, 30290–30296.

55 H. R. Jiang, W. Shyy, M. Liu, L. Wei, M. C. Wu and T. S. Zhao, Boron phosphide monolayer as a potential anode material for alkali metal-based batteries, *J. Mater. Chem. A*, 2017, **5**, 672–679.

56 C. Eames and M. S. Islam, Ion intercalation into two-dimensional transition-metal carbides: global screening for new high-capacity battery materials, *J. Am. Chem. Soc.*, 2014, **136**, 16270–16276.

57 J. Rehman, X. Fan and W. T. Zheng, Computational insight of monolayer SnS_2 as anode material for potassium ion batteries, *Appl. Surf. Sci.*, 2019, **496**, 143625.

58 S. Yi, G. Liu, Z. Liu, W. Hu and H. Deng, Double-layer honeycomb AlP: a promising anode material for Li-, Na-, and K-ion batteries, *J. Phys. Chem. C*, 2020, **124**, 2978–2986.